PHYSICAL REVIEW B 81, 195316 (2010)

Conductance decay of a surface hydrogen tunneling junction fabricated along a Si(001)-(2×1)-H atomic wire

Hiroyo Kawai,[1] Yong Kiat Yeo,[1,2] Mark Saeys,[2,*] and Christian Joachim[1,3,†]

[1]Institute of Materials Research and Engineering, 3 Research Link, Singapore 117602, Singapore

[2]Department of Chemical and Biomolecular Engineering, National University of Singapore, 4 Engineering Drive 4, Singapore 117576, Singapore

[3]Centre d'Elaboration des Materiaux et d'Etudes Structurales (CEMES), CNRS, 29 rue J. Marvig, 31055 Toulouse Cedex, France

(Received 31 December 2009; revised manuscript received 12 April 2010; published 18 May 2010)

On a Si(001)-(2×1)-H substrate, electrons tunneling through hydrogen atomic junctions fabricated between two surface dangling-bond (DB) wires are theoretically investigated using the elastic-scattering quantum-chemistry method. The surface states introduced in the Si band gap by removing H atoms from a Si(001)-(2×1)-H surface were calculated and also analyzed using a simple tight-binding model. The two-channel surface conductance of a DB wire results from a combination of through-space and through-lattice electronic couplings between DB states. The conductance of the DB wire-H-junction-DB wire structure decreases exponentially with the length of H junction with an inverse decay rate ranging from 0.20 to 0.23 $Å^{-1}$, depending on the energy. When the DB wire-H-junction-DB wire structure is contacted by Au nanoelectrodes, the transmission resonances corresponding to the DB wire states split, demonstrating a coupling of the DB wires through short surface hydrogen atomic junctions. This splitting decreases with the length of H junction between the DB wires with an inverse decay length ranging from 0.22 to 0.44 $Å^{-1}$, indicating that such an atomic scale surface tunneling junction is not a very good insulator.

DOI: 10.1103/PhysRevB.81.195316 PACS number(s): 03.65.Xp

I. INTRODUCTION

Fabrication of atomic scale structures has been of great interest due to their potential application in molecular scale electronic devices.[1] It has been shown that such structures can be constructed using the scanning tunneling microscope (STM), which allows the selective removal of surface atoms to create lines and other patterns.[2–7] For example, a surface atomic wire can be formed on a semiconductor surface passivated by an insulating layer. When the insulating layer is removed atom by atom from the surface using the STM tip, the depassivated sites introduce dangling-bond (DBs) states in the band gap, and a line of DBs has a one-dimensional metallic character which can be used as a conducting wire.[8–10] In addition, since the chemical reactivity of DB sites is different from that of passivated sites, the DBs can also be used as a template to form atomic lines by adsorption of, e.g., Ga and Al.[11,12]

The formation of DB lines has been demonstrated on semiconductor surfaces such as MoS_2 (Ref. 2) and Si(001)-(2×1)-H.[4–7] Hosaka *et al.*[2] created patterns on a MoS_2 substrate by removing surface S atoms using the STM tip. Theoretical work by Yong *et al.* showed that the resulting DB wire on MoS_2 introduces localized electronic states within the MoS_2 band gap which create pseudoballistic channels where the conductance does not decrease with the wire length.[8] Among the semiconductor materials, the hydrogen-terminated Si(001)-(2×1)-H surface is of great interest since Si(001) is widely used in semiconductor devices and has been well characterized. The creation of isolated DBs (Ref. 3) as well as lines of DBs (Refs. 4–7) has also been achieved by the removal of H atoms from the surface using the STM tip. Soukiassian *et al.* created a circuitlike pattern on the Si surface by selectively removing H atoms from the surface, showing the preciseness of atomic wire fabrication with STM (Ref. 7) while Hitosugi *et al.*[6] showed experimentally that a line of DBs has a finite density of states near the Fermi energy. Recently, Haider *et al.* showed that a single DB on a hydrogen-terminated silicon Si(001)-(2×1)-H surface can act as a quantum dot where charging and coupling between DBs can be controlled at room temperature to demonstrate the possible creation of atom-scale, quantum dot-based devices.[3]

To characterize the electronic properties of DB wires on a Si(001)-(2×1)-H surface in more detail, several groups have theoretically determined their electronic band structure.[9,10,13–15] Watanabe *et al.*[9] calculated the energy band structure of a DB wire parallel to the Si dimer rows [Fig. 1(a)] using density-functional theory (DFT) and confirmed the introduction of a midgap band by the DB wire. These electronic states could allow electrons to propagate along the DB wire. For comparison, the band structure of the DB wire perpendicular to the dimer rows was also studied. The corresponding midgap band shows a very small dispersion along the wire and therefore a line of DBs in this direction would be less effective for electron propagation.[9]

Although DFT calculations using the generalized gradient approximation (GGA) capture these trends in electronic structure, the results may not be quantitative since the Si band gap is known to be underestimated by DFT-GGA.[16] The semiempirical extended Hückel molecular orbital (EHMO) Hamiltonian[17] provides an alternative to DFT-GGA and can calculate a correct Si band gap when appropriate parameters are used.[18] Moreover, EHMO is computationally more efficient than DFT and is based on Slater type orbitals, which show correct exponential decay of the wave function, important to describe electron tunneling through a junction. Doumergue *et al.* and Raza *et al.* calculated the band struc-

 ©2010 The American Physical Society

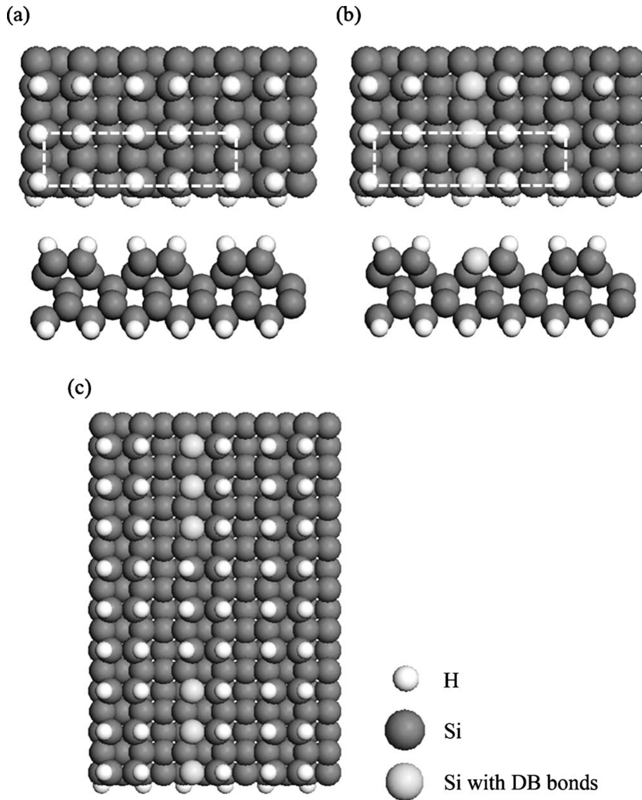

FIG. 1. Atomic structures of the Si(001)-(2×1)-H surface model. (a) Top view and side view of a fully hydrogenated substrate. (b) Top view and side view of a substrate with a DB wire formed by the removal of a line of H atoms. The dotted line shows the corresponding surface supercell for the band structure in Fig. 2. (c) An example of semi-infinite DB wires contacting a three-H atom tunneling junction.

ture of the DB wire parallel to the Si dimer rows using an EHMO Hamiltonian and showed the same qualitative trends as the DFT results for the DB states while matching the experimental Si(001)-(2×1)-H band gap, suggesting the validity of the EHMO Hamiltonian to describe the electronic properties of DBs on a Si(001)-(2×1)-H surface.[10,13]

In addition to the band-structure calculation, Doumergue *et al.* investigated the conductance of a DB wire contacted by two metal electrodes. They fully considered the effect of the underlying surface and of the contacting electrodes, and compared it with the conductance of a fully hydrogenated Si(001)-(2×1)-H surface. Their calculations showed that the conductance of a DB wire does not decrease significantly with length whereas the conductance of a fully hydrogenated substrate decreased with distance between the contact electrodes, further confirming the pseudoballistic character of a DB wire on a hydrogen-passivated Si(001)-(2×1)-H surface.[10]

Though several theoretical studies for surface atomic wires have been published, detailed investigations of an atomic H-tunneling junction contacted by two DB wires [Fig. 1(c)] have not been reported. Understanding the tunneling properties of an atomic junction and its effects on the wire conductance would be important to begin to apply and design surface DBs for molecular electronic interconnection[1] and for atomic scale devices such as surface atomic logic gates. In the present work, the properties of an atomic H-tunneling junction contacted by DB wires and created on a hydrogen-passivated Si(001)-(2×1)-H surface are explored theoretically. The model for a fully passivated Si(001)-(2×1)-H surface and for the substrate with a line of DBs are shown in Figs. 1(a) and 1(b), respectively. The H-tunneling junction is created by leaving H atoms between sections of the DB wire and the length of the H junction can be varied by increasing the number of H atoms. An example of three-H atom long junction is shown in Fig. 1(c). The objective of this work is to investigate the mechanism of electron propagation along the surface DB wire and through the H junction. This paper is divided into several sections. First, the atomic and electronic band structures of a DB wire on a Si(001)-(2×1)-H substrate are discussed, followed by the characterization of electron transmission along a DB wire. Then the H-tunneling junction is introduced into the DB wire and its effect on the electron transport along the wire is determined. To analyze and explain the electron transmission properties for each case, a tight-binding model of the DB wire and of the junction is also developed. Finally, the electronic insulating properties of an atomic surface H-tunneling junction are analyzed in detail.

II. ATOMIC AND ELECTRONIC BAND STRUCTURES FOR DB WIRES

An accurate description of the electronic band structures of the substrate is important to characterize the electron-transport properties of a DB wire and a H-tunneling junction. In our calculations, the Si(001)-(2×1)-H surface was modeled as a five-layer silicon slab, and the DB wire on the surface was formed by removing a row of H atoms along a dimer row [Fig. 1(b)]. The atomic structure of a hydrogen-terminated silicon surface studied in this work was referenced from the work by Doumergue *et al.*[10] and Watanabe *et al.*,[9] where the geometries of the top three layers of Si were optimized using the conjugate gradient method to obtain a reconstructed 2×1 surface. The relaxation of the surface atoms upon removal of H atoms was neglected because according to Watanabe *et al.*, the position of the Si atom without a H atom was lowered only by 0.1 Å.[9] The electronic band structure of the substrate was described using the EHMO Hamiltonian.[17] The advantage of EHMO approach over DFT, as mentioned earlier, is that it provides an accurate band gap, is computationally more efficient, and becomes practical to model more complex systems such as the metal electrode-atomic wire-metal electrode junction studied here. In addition, the EHMO Hamiltonian can be easily incorporated into the subsequent electron-transport calculations.

The band structures of the Si(001)-(2×1)-H surface with and without the DB wire, calculated using EHMO and DFT methods are shown in Fig. 2. The surface supercells used in the calculations for each structure are shown in Figs. 1(a) and 1(b). Bulk silicon EHMO parameters for a *spd* basis set have been determined by Kienle *et al.*[18] and can be used to describe silicon surfaces. However, to calculate electron transport in a complex system such as atomic junctions stud-

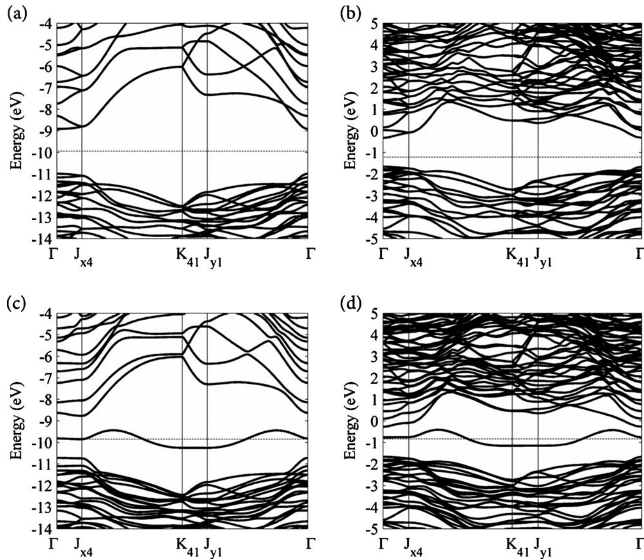

FIG. 2. Energy band structures for a fully hydrogenated Si(001)-(2×1)-H surface, calculated with (a) EHMO and (b) DFT-PBE methods, and energy band structures for the Si(001)-(2×1)-H surface with a DB wire, calculated with (c) EHMO and (d) DFT-PBE methods, along the symmetry axis of the supercell shown in Fig. 1. The position of the Fermi energy is indicated by a dotted line.

ied here, the computational requirement increases significantly with the number of atomic orbitals in the basis set. Therefore, we chose to reduce the number of orbitals and use a *sp* instead of a *spd* basis set. The parameters for the s and p orbitals from Kienle *et al.*'s EHMO Hamiltonian were reparametrized to match the DFT band structure for the DB wire and the experimental band gap for the Si(001)-(2×1)-H surface. The EHMO band structures were calculated using the BICON-CEDIT program.[19] DFT band structures were obtained using the Vienna *ab initio* simulation package with the Perdew-Burke-Ernzerhof (PBE) (Ref. 20) functional and the projector-augmented wave method.[21]

The EHMO and DFT band gap for the hydrogenated Si(001)-(2×1)-H surface of 2.08 eV and 1.34 eV, respectively, can be compared to the experimental surface gap of about 2.0 eV.[7] The EHMO band gap is also consistent with a previous EHMO calculation by Doumergue *et al.*[10] The DB wire on the Si(001)-(2×1)-H surface has a wire band located within the surface gap, resulting from the DB states [Figs. 2(c) and 2(d)]. The EHMO and DFT energy dispersion for the wire band are 0.82 eV and 0.74 eV, respectively. The EHMO dispersion is somewhat larger, consistent with the larger band gap, but the shape of the DB-derived band agrees qualitatively with the DFT-PBE band, as well as with the DFT band reported by Watanabe *et al.*[9] The band shape is also consistent with the previous EHMO results by Doumergue *et al.*[10] and by Raza.[13]

Although the description of the DB wire band by EHMO theory is comparable to DFT-PBE, there are minor differences in the conduction band caused by the absence of *d* orbitals in our EHMO Hamiltonian. Kienle *et al.*[18] used *spd* orbitals model to calculate the band structure of bulk Si and of the reconstructed Si(001) surface and found good agree-

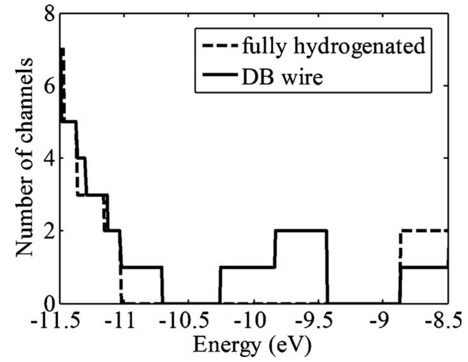

FIG. 3. Number of conduction channels along the dimer row for a fully hydrogenated substrate (dotted line) and for a substrate with a DB wire (solid line). Conduction channels exist within the gap for the substrate with a DB wire, consistent with the band structure in Fig. 2(c).

ment for both valence and conduction bands. However, the *sp* orbitals model is sufficient to explore electron propagation along a DB wire.

III. THROUGH-SPACE AND THROUGH-LATTICE COUPLINGS BETWEEN DB STATES

The properties of electron propagation along a DB wire were determined using the EHMO electronic structures described in Sec. II. In previous studies,[10] the band structure and conductance of a DB wire were attributed to through-space coupling of the DB states consisting of surface Si p_z orbitals, similar to the situation for polyene molecular wires.[22] However, the wire band structure runs both up and down and hence cannot be described by through-space coupling between the DB p_z orbitals alone. Indeed, the band structure and the conductance of a DB wire result from a combination of through-space and through-lattice electronic couplings. The importance of both couplings was explored by calculating the number of conduction channels for an infinite DB atomic wire using the elastic-scattering quantum-chemistry (ESQC) method,[23] and by developing a tight-binding model to interpret the ESQC results and explain electron propagation in this structure.

ESQC uses a linear combination of atomic orbitals EHMO Hamiltonian for each subsystem to describe the interactions within and between the subsystems.[23] Doumergue *et al.*[10] calculated electron-transport properties for finite atomic wires on a Si(001)-(2×1)-H surface using the same approach but in our calculations, the EHMO model was reparametrized to describe the dispersion and shape of the DB wire band as well as its location relative to the valence band. In Fig. 3, the number of conduction channels is plotted as a function of the electron energy for the fully hydrogenated surface and for the surface with a DB wire. In both cases, the system is periodic in the direction of the DB wire. The number of channels reflects the number of propagating Bloch states for each energy value and can be equal to or greater than one in the conduction band and in the valence-band region. Without the DB wire, the number of channels in the band-gap region is zero. The DB wire introduces conduction

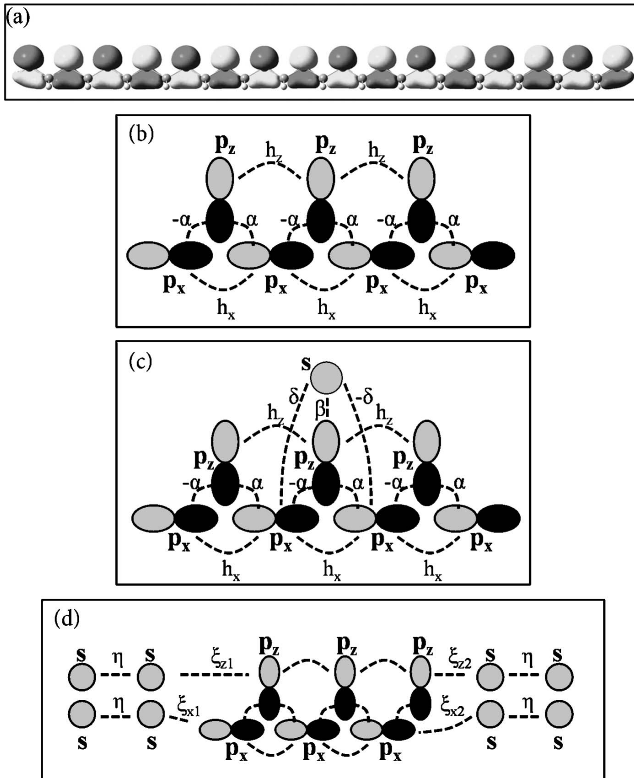

FIG. 4. (a) Lowest energy molecular orbital for a 16-DB Si chain model. (b) Tight-binding model for a DB wire created on the Si(001)-(2×1)-H surface. Each unit cell is composed of p_x and p_z orbital coupled through α, and linked to adjacent cells by h_z, h_x, and α couplings. Adjacent same color corresponds to a negative coupling and conversely, adjacent opposite color corresponds to a positive coupling. (c) Tight-binding model for a H-tunneling junction contacted by two semi-infinite DB wires. The unit cell is composed of p_x, p_z, and s orbitals coupled by α and β, respectively, and is linked to adjacent cells by h_x, h_z, α, and δ couplings. (d) Tight-binding representation of a DB wire coupled to two semi-infinite Au electrodes. The model is equivalent to (b) except that each end of the DB wires is coupled to two s orbitals of the metal electrodes.

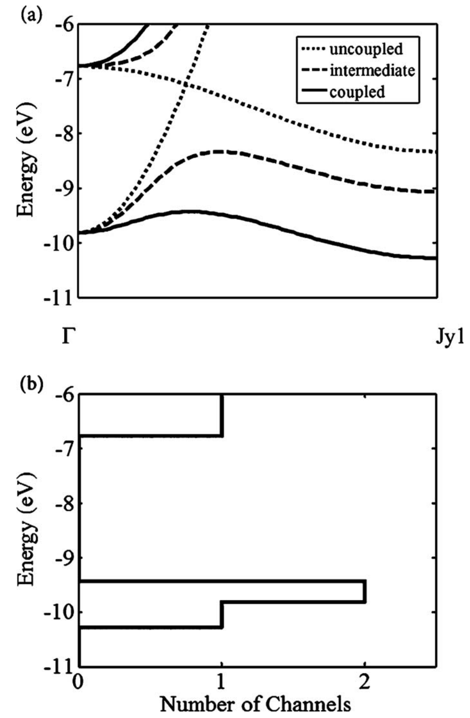

FIG. 5. (a) Tight-binding band structure for the DB-derived band along a DB wire (Γ-J_{y1}). The dotted lines show the uncoupled p_x and p_z bands (α=0 eV). The dashed and solid lines show the bands when p_x and p_z are weakly coupled (α=1.50 eV) and strongly coupled (α=2.56 eV), respectively. (b) Number of conduction channels along a DB wire for the tight-binding model.

channels within the band gap and around the Fermi level, corresponding with the DB wire-derived band [Fig. 2(c)]. There are two channels between −9.8 and −9.4 eV and one channel between −9.8 and −10.2 eV. The DB band structure [Fig. 2(c)] also indicates that there are two propagating Bloch waves at different k values between −9.8 and −9.4 eV.

To elucidate the character of the propagating Bloch waves, the molecular orbitals (MOs) for a chain of fully hydrogenated Si atoms were obtained using GAUSSIAN03 (Ref. 24) and the effect of removing one H atom per surface Si atom was evaluated [Fig. 4(a)]. The DFT-PBE (Ref. 20) method was used with a 6-31G(d,p) basis set. Initially, when all the bonds of Si are saturated, the energy levels are separated by an energy gap. One state is introduced in the gap region each time a surface H atom is removed.[9,10] If the p_z-type DB states interact only through space, then the bonding combination would be the most stable MO and the antibonding combination would be the least stable.[25] Instead, the most stable DB wire MO is the antibonding combination of the surface p_z orbitals coupled through the Si lattice via p_x orbitals of the subsurface Si atoms [Fig. 4(a)] and the bonding combination has intermediate stability. Therefore, to model the conductance of a DB atomic wire on the Si(001)-(2×1)-H surface, both through-space and through-lattice couplings need to be considered.

A tight-binding model with two levels per DB was constructed to simulate the band structure for an infinite DB wire [Fig. 4(b)]. The DB p_z levels in adjacent cells are coupled through space by a negative coupling integral h_z and through lattice via the subsurface Si p_x orbitals. The through-lattice coupling integral α alternates between positive and negative values due to the symmetry of the p_z and p_x orbitals. The p_x levels in adjacent cells are coupled via a positive coupling integral h_x. Figure 5(a) illustrates the effect of the through-lattice coupling on the band structure. Through-lattice coupling has the largest effect for k values near J_{y1}, where the p_z-p_z interactions are antibonding and p_x-p_z interactions are bonding. Near the Γ point, through-space coupling is dominant. Because the DB band runs both up and down in k space, a maximum of two propagating channels can be found. With the six coupling parameters, the tight-binding band can be fitted accurately to the EHMO band. The number of conduction channels for the DB wire corresponds with the band structure [Fig. 5(b)].

IV. CONDUCTANCE OF A SHORT DB WIRE

On a Si(001)-(2×1)-H surface and fabricated by vertical STM H-atom manipulation, a DB wire will certainly have a

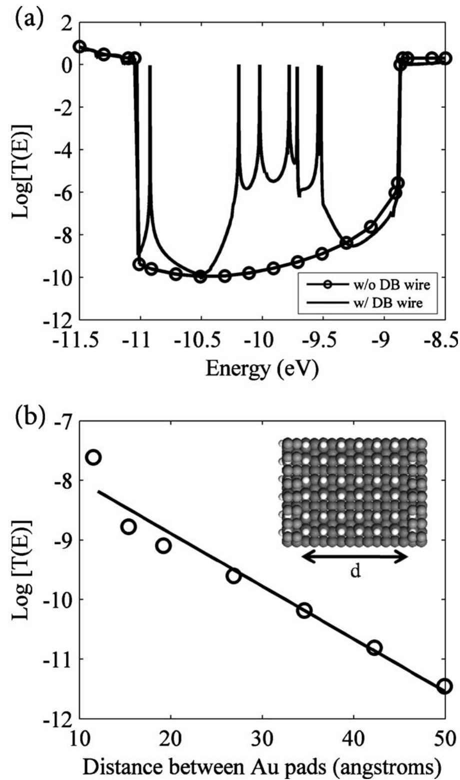

FIG. 6. (a) Calculated transmission spectrum for a fully hydrogenated Si(001)-(2×1)-H surface without DB wire between two Au electrodes (circles) and $T(E)$ spectrum for a surface with a finite DB wire contacted by Au electrodes (solid line). The distance between the two Au electrodes is 27 Å (six Si dimers). (b) Semilogarithmic plot of the transmission decay for a fully hydrogenated surface as a function of the distance between the Au electrodes at the Fermi energy (−9.9 eV). The inverse decay length, γ, is about 0.20 Å^{-1}. The surface model for a substrate with Au electrodes is also shown.

finite length and be contacted by metallic nanoelectrodes. We have studied the effect of the DB wire length and of the contacting nanoelectrodes on its ballistic transport properties. In ESQC, this can be modeled by adding semi-infinite gold nanoelectrodes on the hydrogenated Si(001)-(2×1)-H surface [Fig. 6(b) inset] and by introducing a finite line of DBs between them. The junctions conductances were calculated to compare with the results by Doumergue *et al.*[10] because of the better surface band-structure optimization performed here.

The $T(E)$ spectrum of an insulating junction without a DB wire was calculated first. The $T(E)$ values are very low in the energy band gap of the surface as shown by the dotted line in Fig. 6(a). The energy range of this gap corresponds well with the calculated band structure in Fig. 2(a). In the center of the gap, the decrease in $T(E)$ as a function of the distance d between the Au nanoelectrodes can be described by

$$T(d) = T_0 e^{-\gamma d}, \tag{1}$$

as also used to describe the conductance decay of various atomic[26] and molecular wires[22,27] with length. γ is the inverse decay length and for the Si(001)-(2×1)-H surface with two Au nanoelectrodes, d is the distance between these nanoelectrodes in angstrom. For a fully passivated substrate, the inverse decay length is about 0.20 Å^{-1} at the −9.9 eV Fermi energy [Fig. 6(b)]. This is smaller than the value of 0.41 Å^{-1} calculated by Doumergue *et al.* The difference arises from the fact that the effective mass $m^*(E)$ of an electron tunneling through a barrier controls the inverse decay length,[28]

$$\gamma(E) = \sqrt{\frac{2m^*(E)}{\hbar^2}\frac{(E-E_v)(E_c-E)}{\chi}}, \tag{2}$$

where E is the electron energy, $\hbar$ is Planck's constant, χ is the band gap, and E_v and E_c are valence-band and conduction-band edges, respectively. $m^*(E)$ is very sensitive to the nature of the electronic band structures used. Thus, although χ in our model is comparable to that of Doumergue *et al.*, the difference between our band structure, supported by DFT calculations, and the band structure reported by Doumergue *et al.* accounts for the difference in $m^*(E)$ at the Fermi energy and therefore in γ.

The $T(E)$ spectrum for a finite wire of six DBs between two Au nanoelectrodes is shown in Fig. 6(a). Resonance peaks resulting from the DBs states appear within the energy range of the infinite wire band. Note that the resonances come in pairs for the two-channel region. This pairing of the peaks becomes more apparent for a longer DB wire. Figure 7(a) shows the transmission spectrum for a ten-DB wire between the Au electrodes. There are four peaks in the one-channel energy range and three pairs of peaks in the two-channel energy range. The peaks in each pair are asymmetric, as shown in the inset of Fig. 7(a). In addition to the peaks in the wire band region, a single resonance peak also appears near the valence-band edge. This resonance results from the building up of a band at the top of the valence band in the EHMO model [Fig. 2(c)].

To further analyze the metal-DB wire-metal junction, the gold nanoelectrodes were also simulated in the tight-binding model described in Sec. III. An s-wave propagator with two channels was constructed, one channel being weakly coupled to the p_z orbital of the DB closest to the Au nanoelectrode and the second channel to the p_x orbital of the DB closest to the nanoelectrode [Fig. 4(c)]. Sufficiently large coupling integrals were used for the gold nanoelectrodes to create a wide incoming and outgoing band. This tight-binding model describes the monoelectronic properties of a quantum box like system where the nanoelectrodes are elastically supplying and withdrawing electrons to and from the box over a wide energy range. For a wire of ten DBs and similar to the ESQC spectrum, the tight-binding model shows two groups of peaks, one group corresponding to states close to the Γ point of the infinite wire band for the through-space coupling and one group corresponding to the other part of the band structure for the through-lattice coupling. Each group leads to a separate $T(E)$ envelope [Fig. 7(b)]. The peaks appear as asymmetric pairs in the two-channel energy range. This asymmetry can be related to the difference in coupling between the p_z and Au nanoelectrode propagator on the one hand, and between the subsurface p_x orbitals and the Au

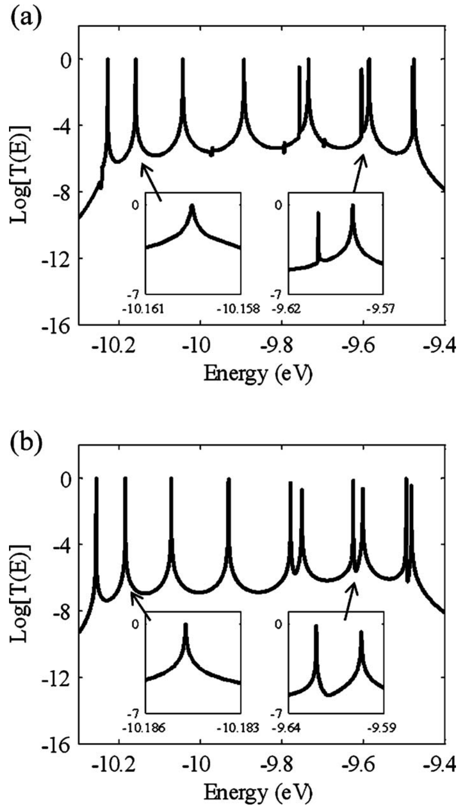

FIG. 7. Transmission spectrum for a Au electrode-DB wire-Au electrode junction with a wire length of 42 Å (ten DBs), calculated (a) using the ESQC method and (b) using the tight-binding model. The insets zoom in on selected peaks. In the lower energy range (the one-channel region) each peak is well separated while in the higher energy range (the two-channel region), the peaks come in pairs.

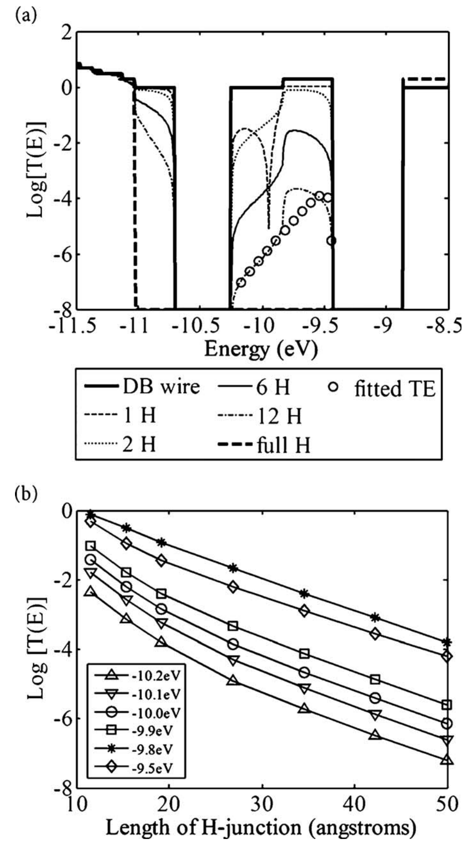

FIG. 8. (a) Transmission spectra for H junctions contacted by semi-infinite DB wires. The transmission spectrum for an infinite DB wire and for the fully hydrogenated Si(001)-(2×1)-H surface are also shown. See Fig. 1(c) for the atomic structure. Empty circles show the transmission spectrum fitted to the 12-H junction using the one-channel model (Sec. VII). (b) Semilogarithmic plots of the transmission decay with increasing H-junction size at different energies. At the Fermi energy (−9.9 eV) $T(E)$ decreases exponentially with an inverse decay length of 0.22 Å^{-1} for junctions greater than 25 Å.

nanoelectrode propagator on the other. In the tight-binding model, the peaks in each pair are somewhat closer compared to the peaks in the complete EHMO ESQC simulations.

With a tight-binding model, it is easy to compute the transmission spectrum for very long wires coupled to simulated Au nanoelectrodes at both sides and to model the gradual transition in $T(E)$ from a short wire to an infinite wire. This allows visualizing how a band builds up in the two-channel regime. For a single channel, it has already been shown that when the number of states in the central wire increases, the various resonance peaks converge to a parabola-shaped envelope with a maximum $T(E)=1$ for an optimal coupling between the finite wire and the semi-infinite electrodes.[8] The transmission increases gradually with the coupling between the DB wire and the Au nanoelectrodes to reach a maximum value of 1 at the resonance peaks. When the coupling is further increased, the overall transmission decreases due to overcoupling.[8,23] In the two-channel energy range, the $T(E)$ resonances build up smoothly as a function of the wire length to pass over unity as the separate envelopes of peaks overlap at well-defined energies and to converge toward $T(E)=2$ when the coupling between the wire and the nanoelectrodes is also well balanced.

V. ATOMIC WIRES CONTACTING A SURFACE H-TUNNELING JUNCTION

In this section, the electronic transparency of a surface H-tunneling junction consisting of n hydrogenated DBs, contacted by semi-infinite DB wires [Fig. 1(c)], is discussed. The $T(E)$ spectra for different H-junction lengths are shown in Fig. 8(a). For H junctions longer than one H atom, the $T(E)$ decreases exponentially with the length of the H junction [Fig. 8(b)] in the energy range of the central band. At the Fermi energy, the inverse decay length $\gamma=0.22$ Å^{-1} is comparable to the value calculated for the Au nanoelectrode-Si(001)-(2×1)-H-Au nanoelectrode junction discussed in Sec. IV and it varies from 0.20 Å^{-1} for energies near the top of the wire band to 0.23 Å^{-1} near the bottom of the band [Fig. 8(b)]. For short H junctions less than 25 Å, γ ranges from 0.44 Å^{-1} near the top of the wire band to 0.34 Å^{-1} near the bottom of the band and are larger than for long H junctions. This is because it requires more than four H atoms to build up a conduction bandlike structure corresponding to the H-tunneling junction. Introducing less than

four H atoms creates junction-induced states that are higher in energy than the conduction-band edge corresponding to a long H junction, in turn leading to a faster decay rate, γ. The γ for a short H junction will be discussed again in Sec. VII.

The $T(E)$ spectrum for a one H junction differs qualitatively from the $T(E)$ for a longer H junctions because introducing a single H atom eliminates only one of the channels in the two-channel range but leaves the other channel unaffected. As a consequence, in the one-channel energy range at $E=-9.94$ eV, a destructive interference is obtained. This is well simulated with our tight-binding model where the H junction is modeled by coupling a single H level to both the DB p_z level and the lattice p_x levels via β and δ electronic couplings, respectively [Fig. 4(c)]. The position of the destructive interference in the $T(E)$ spectrum is controlled by both β and δ. Our tight-binding model also reproduces the removal of one of the channels in the two-channel energy range upon introduction of a single H atom. Indeed, the lattice channel is very sensitive to the interaction with a H atom. This is consistent with the change in the wire band near J_{y1} [Fig. 5(a)] when coupled to the DB states. From the parameters derived in Sec. IV, the γ ranges from 0.32 Å^{-1} near the top of the wire band to 0.40 Å^{-1} near the bottom of the band with tight-binding model, compared to 0.20 and 0.23 Å^{-1} from the ESQC results, and they are reasonably consistent. The discrepancy is attributed to the fact that only a few orbitals are represented in the tight-binding model, contributing to a faster rate of decay.

VI. CONDUCTANCE OF AN ELECTRODE-WIRE-JUNCTION-WIRE-ELECTRODE SYSTEM

Similar to H junctions constructed experimentally using STM,[29] a complete surface tunnel junction consisting of a H-tunneling junction inserted between two short DB wires and contacted by semi-infinite Au nanoelectrodes was considered. As discussed in Sec. III, a $T(E)$ spectrum for a finite length DB wire consists of a series of resonance peaks. When two finite length DB wires are interacting through a H junction, each resonance peak splits with a splitting energy depending on the electronic coupling through the H junction. For a small H-junction, this coupling is strong enough to be observable in the $T(E)$ spectrum. A series of double-resonance peaks is obtained, reflecting the resonances of the two DB wires. As the length of the H junction increases, the two DB wires are progressively decoupled and the resonance peaks gradually converge. Finally, for very long H junctions, the splitting becomes smaller than the width of each individual $T(E)$ peak. In this case, the $T(E)$ spectrum resembles the spectrum of a single DB wire. To illustrate this, the ESQC $T(E)$ spectra of a one H junction and of a four H junction, both contacted by two four-DB-long wires were calculated (Fig. 9). For comparison, the corresponding $T(E)$ for the tight-binding models of those two junctions were also calculated, showing a similar splitting phenomenon (not shown).

The inverse decay length γ of a H junction can now be calculated by following the effect of the length of the H junction on the energy splitting for each resonance peak. In Fig. 10(a), the splitting for each resonance peak is shown as a function of the length of the H junction. To compare with the γ obtained for the semi-infinite DB wire-H-junction-DB wire junction (Sec. IV), a factor 2 must be used.[23] The calculated decay length γ is slightly different for each resonance and depends on their energy position: 0.44 Å^{-1}, 0.27 Å^{-1}, 0.22 Å^{-1}, and 0.33 Å^{-1} at the energy of −10.13 eV, −9.85 eV, −9.64 eV, and −9.56 eV, corresponding to the first, second, third, and fourth pair, respectively.

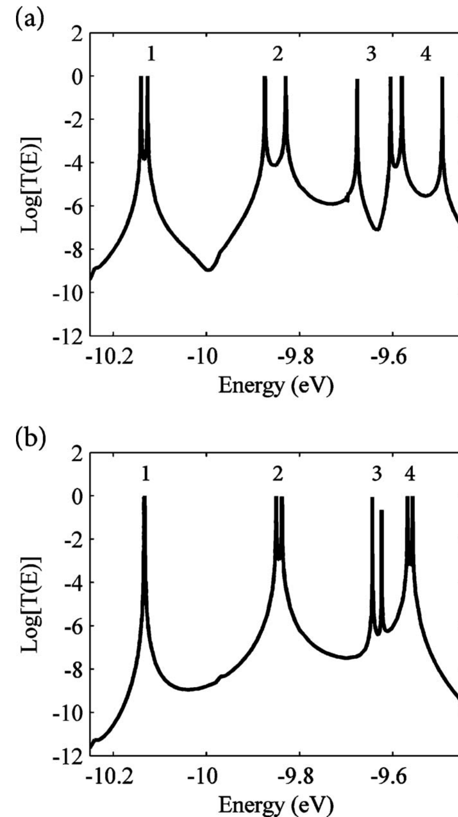

FIG. 9. Transmission spectrum (a) for a four DB-one H-four DB junction and (b) for a four DB-four H-four DB junction contacted by two Au electrodes. The resonance peaks appear in pairs because the two short DB wires retain a degree of coupling through the H junction. The energy at pair 1, 2, 3, and 4 are located at −10.13 eV, −9.85 eV, −9.64 eV, and −9.56 eV, respectively. The tight-binding transmission spectra (not shown) are similar to the ESQC spectra.

VII. DISCUSSION

Three different surface atomic H junctions have been considered: a fully passivated Si(001)-(2×1)-H surface contacted by two Au nanoelectrodes (Sec. IV), a H junction contacted by two semi-infinite DB wires (Sec. V), and a H junction located in between two short DB wires each contacted by an Au nanoelectrode (Sec. VI). Each surface H junction acts as a potential energy barrier for the electrons traveling ballistically from one electrode to the other. There-

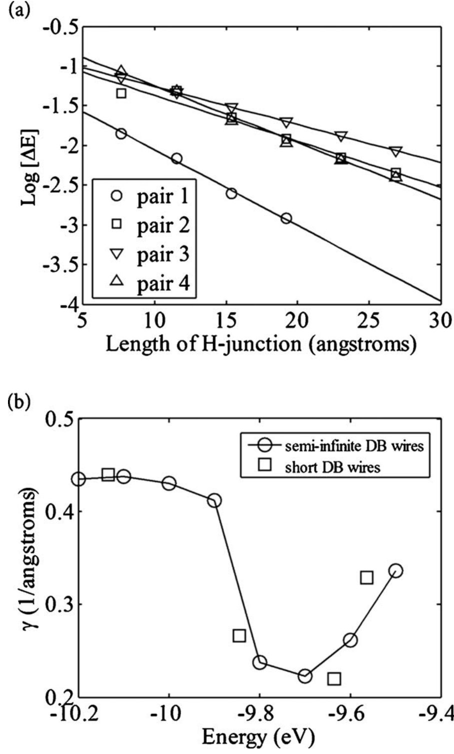

FIG. 10. (a) Semilogarithmic plot of the energy splitting between two peaks as a function of the length of a short H junction for each pair. For the four-DB wire, there are four pairs of peaks, where pair 1 is located at lowest energy and pair 4 is at highest energy (Fig. 9). (b) Inverse decay length γ calculated for short H junctions contacted by two semi-infinite DB wires [Fig. 8(b)] and calculated from the energy splitting for short H junctions between short DB wires [Fig. 10(a)].

fore, the tunneling transmission coefficient decays with the length of the H junction.

The electronic band structure of a fully passivated Si(001)-(2×1)-H surface contacted by two Au nanoelectrodes presents a parabolic tunneling band in the complex plane, linking the surface valence and conduction bands. This type of complex band structure has been explored previously.[30] More recently, it was used to derive an analytical expression for the inverse decay length γ as a function of the characteristics of the complex band structure [see also Eq. (2) in Sec. IV].[28] For a long surface H junction contacted by long DB wires, however, the wire band of the incoming electrons lies fully within the band gap of the H junction, resulting in an energy gap between the top of the valence-band edge and one below the bottom of the surface conduction band. In this case, the complex parabolic band structure corresponding to the H junction is not directly connected to the incoming wire band. In fact, in this case the parabola is reversed and the complex band structure presents a sharp discontinuity at each edge of the DB wire band, as demonstrated in Sec. III. In this case, γ can be fitted by generalized expression,[31]

$$\gamma(E) = \sqrt{\frac{2m^*(E)}{\hbar^2}\frac{(E_c - E_h)(E_h - E_l)(E_l - E_v)}{(E_c - E)(E - E_v)}}, \qquad (3)$$

accounting for the complex surface band structure created by the DB wires and the H junction. In Eq. (3), E_v and E_c are the energies of valence-band and conduction-band edges, and E_h and E_l are the energies of the top and bottom of the DB wire central band structure. In the one-channel energy range, the decay of the $T(E)$ spectrum with the length of the junction can be described by Eq. (3) as presented in Fig. 8(a) with the circle curve. There are some deviations from Eq. (3) in the two-channel energy range and further studies are required to derive a generalization of Eq. (3) for this case. As a consequence of Eq. (3), γ is not constant over the full energy range of the DB wire band structure. It is possible to estimate $m^*(E)$ for the one- and two-channel regimes but this is beyond the scope of this work.[31]

When the H junction is contacted by two short DB wires, the overall tunneling decay is a convolution of the DB wire properties and the characteristics of the atomic H junction. To address the properties of the H junction independently, the $T(E)$ decay is related to the splitting of the resonance peaks. Again, γ is a function of energy and a different value is obtained for each pair. The decay length γ obtained for a H junction contacted by semi-infinite DB wires [Fig. 8(b)] and the γ obtained from the splitting of the resonance peaks are compared in Fig. 10(b). Note that in this case the junctions are short and therefore the values of γ are different from the values for longer junctions, as discussed in Sec. V. In addition, γ is a strong function of energy, where its value is larger for the one-channel energy range than for the two-channel range [Fig. 10(b)].

A surface H junction can also be simply modeled as a square potential energy barrier where the transmission coefficient decays exponentially with the barrier height and width. The potential barrier height indicates how the surface H junction acts as an insulating electronic barrier decoupling the two DB wires. In this simple model, one can always relate γ to an effective barrier height Φ by the simple Wentzel-Kramers-Brillouin expression,[32]

$$\gamma(E) = \sqrt{\frac{2m^*(E)\Phi}{\hbar^2}}, \qquad (4)$$

where $m^*(E)$ is the effective mass of the tunneling electrons. Using an $m^*(E)$ estimated from Eq. (3), one can find $\Phi = 0.3$ eV at $E = -10$ eV. According to our calculations, a H junction must then be at least 27 Å (six H atoms) long to significantly weaken the electronic coupling between the two contacting DB wires and to decrease the $T(E)$ by two orders of magnitude. Therefore, a H junction on an Si(001)-(2×1)-H surface is not a very effective insulating barrier, e.g., as compared to an SiO_2 barrier which has a γ of about 1.2 Å^{-1}.[33]

VIII. CONCLUSIONS

We have theoretically analyzed the ballistic electron-transport properties along a DB wire and across an atomic H

junction created on a Si(001)-(2×1)-H surface using the ESQC method and using a tight-binding model. The analysis shows that the electronic structure of a DB wire results from a combination of through-space and through-lattice couplings of the DB p_z orbitals, and the combination of both couplings explains the different features observed in the calculated electronic transmission spectra. The transparency of atomic H junctions located along a DB wire was calculated. Three different H-junction configurations have been considered: a H junction contacted by two semi-infinite DB wires, a H junction contacted by two semi-infinite Au nanoelectrodes, and a H junction contacted by two finite DB wires which are contacted by Au nanoelectrodes. We found that the inverse decay length is a function of energy, with a higher inverse decay length for the one-channel region of the DB wire band. So far the detailed experimental studies on the electron tunneling across the DB wire on Si(001)-(2×1)-H have not been done but the simulation results in this work will certainly guide the experiments. For example, using the knowledge of the DB wire characteristics, we can design more complex atomic scale circuits on the surface with logic gates, and the circuits can then be fabricated and tested experimentally.[29] Although there are other potential challenges such as the current leakage within such device, our work is a step toward the designing of atomic scale circuits and will facilitate the future experimental work.

*chesm@nus.edu.sg
†joachim@cemes.fr

[1] C. Joachim, J. K. Gimzewski, and A. Aviram, Nature (London) **408**, 541 (2000).
[2] S. Hosaka, S. Hosoki, T. Hasegawa, H. Koyanagi, T. Shintani, and M. Miyamoto, J. Vac. Sci. Technol. B **13**, 2813 (1995).
[3] M. B. Haider, J. L. Pitters, G. A. DiLabio, L. Livadaru, J. Y. Mutus, and R. A. Wolkow, Phys. Rev. Lett. **102**, 046805 (2009).
[4] J. W. Lyding, T.-C. Shen, J. S. Hubacek, J. R. Tucker, and G. C. Abeln, Appl. Phys. Lett. **64**, 2010 (1994).
[5] T. Hallam, T. C. G. Reusch, L. Oberbeck, N. J. Curson, and M. Y. Simmons, J. Appl. Phys. **101**, 034305 (2007).
[6] T. Hitosugi, T. Hashizume, S. Heike, Y. Wada, S. Watanabe, T. Hasegawa, and K. Kitazawa, Appl. Phys. A: Mater. Sci. Process. **66**, S695 (1998).
[7] L. Soukiassian, A. J. Mayne, M. Carbone, and G. Dujardin, Surf. Sci. **528**, 121 (2003).
[8] K. S. Yong, D. M. Otalvaro, I. Duchemin, M. Saeys, and C. Joachim, Phys. Rev. B **77**, 205429 (2008).
[9] S. Watanabe, Y. A. Ono, T. Hashizume, and Y. Wada, Phys. Rev. B **54**, R17308 (1996).
[10] P. Doumergue, L. Pizzagalli, C. Joachim, A. Altibelli, and A. Baratoff, Phys. Rev. B **59**, 15910 (1999).
[11] J. Nogami, in *Atomic and Molecular Wires*, NATO Advanced Studies Institute Series E: Applied Sciences Vol. 341, edited by C. Joachim and S. Roth (Kluwer, Dordrecht, 1997), p. 11.
[12] T. Hashizume, S. Heike, M. I. Lutwyche, S. Watanabe, K. Nakajima, T. Nishi, and Y. Wada, Jpn. J. Appl. Phys., Part 2 **35**, L1085 (1996).
[13] H. Raza, Phys. Rev. B **76**, 045308 (2007).
[14] H. Raza, T. Z. Raza, and E. C. Kan, Phys. Rev. B **78**, 193401 (2008).
[15] M. Çakmak and G. P. Srivastava, Surf. Sci. **532-535**, 556 (2003).
[16] G. P. Srivastava, *Theoretical Modeling of Semiconductor Surfaces* (World Scientific, River Edge, NJ, 1999).
[17] R. Hoffmann, J. Chem. Phys. **39**, 1397 (1963).
[18] D. Kienle, K. H. Bevan, G.-C. Liang, L. Siddiqui, J. I. Cerda, and A. W. Ghosh, J. Appl. Phys. **100**, 043715 (2006).
[19] M. Brandle, R. Ruedi, and G. Calziferri, BICON-CEDIT, University of Berne, 1997.
[20] J. P. Perdew, K. Burke, and M. Ernzerhof, Phys. Rev. Lett. **77**, 3865 (1996).
[21] G. Kresse and J. Hafner, Phys. Rev. B **47**, 558 (1993).
[22] M. Magoga and C. Joachim, Phys. Rev. B **56**, 4722 (1997).
[23] P. Sautet and C. Joachim, Phys. Rev. B **38**, 12238 (1988).
[24] M. J. Frisch *et al.*, GAUSSIAN 03, Revision C.02, Gaussian, Inc., Wallingford, Connecticut, 2004.
[25] R. Hoffmann, *Solids and Surfaces: A Chemist's View of Bonding in Extended Structures* (Wiley, New York, 1989), pp. 3–10.
[26] L. Pizzagalli, C. Joachim, X. Bouju, and C. Girard, Europhys. Lett. **38**, 97 (1997).
[27] V. Mujica, M. Kemp, and M. A. Ratner, J. Chem. Phys. **101**, 6856 (1994).
[28] C. Joachim and M. Magoga, Chem. Phys. **281**, 347 (2002).
[29] C. Joachim, D. Martrou, M. Rezeq, C. Troadec, D. Jie, N. Chandrasekhar, and S. Gauthier, J. Phys.: Condens. Matter **22**, 084025 (2010).
[30] W. Franz, in *Handbook of Physics*, edited by S. Flügge (Springer, New York, 1956), Vol. 17, p. 155.
[31] Y. K. Yeo, H. Kawai, M. Saeys, and C. Joachim (unpublished).
[32] C. B. Duke, *Tunneling in Solids* (Academic, New York, 1962).
[33] M. L. Green, T. W. Sorsch, G. L. Timp, D. A. Muller, B. E. Weir, P. J. Silverman, S. V. Moccio, and Y. O. Kim, Microelectron. Eng. **48**, 25 (1999).